Characterisation of a fibre optic Raman probe within a hypodermic needle

Ingeborg E. Iping Petterson,[1,2] John C.C. Day,[2] Leanne M. Fullwood,[1,3] Benjamin Gardner,[1] Nick Stone[1,3*]

[1]Biomedical Physics, School of Physics and Astronomy, University of Exeter, Exeter, Devon, EX4 4QL, UK
[2]Interface Analysis Centre, H.H. Wills Physics Laboratory, University of Bristol, Tyndall Avenue, Bristol, BS8 1TL, UK
[3] Biophotonics Research Unit, Gloucestershire Hospitals NHS Foundation Trust, Great Western Road, Gloucestershire, GL1 3NN, UK

Abstract

Here we demonstrate the first use of a multifibre Raman probe that fits inside the bore of a hypodermic needle. A Raman probe utilising multiple collection fibres provides improved signal collection efficiency in biological samples compared with a previous 2-fibre design. Furthermore, probe performance (signal-to-noise ratios (SNRs)) compared favourably with those achieved in previous Raman microscope experiments able to distinguish benign, primary malignancies and secondary malignancies in lymph nodes.

Experimental measurements presented in this paper give an indication of the sampling volume of the Raman needle probe in lymphoid tissues. Liquid tissue phantoms were used, containing scattering media encompassing a range of scattering properties similar to a variety of tissue types, including lymph node tissues. To validate the appropriateness of phantoms, the sampling depth of the probe was also measured in excised lymph node tissue. Greater than 50% of Raman photons collected were found to originate between the tip of the needle and a depth of 500 μm into the tissue.

The needle probe presented here achieves comparable spectral quality to numerous studies previously demonstrating Raman disease discrimination. It is expected that this approach could achieve targeted subcutaneous tissue measurements and be viable for use for the in vivo Raman diagnostics of solid organs located within a few cm below the skin's surface.

Keywords: non-invasive, diagnostics, needle, Raman spectroscopy, lymph nodes

Address all correspondence to: Nick Stone, Biomedical Physics, School of Physics and Astronomy, Stocker Road, University of Exeter, Exeter Devon, EX4 4QL, UK; Tel: (+44)(0)1392 726531; E-mail: N.Stone@exeter.ac.uk

Introduction

Raman spectroscopy is a vibrational spectroscopic technique that provides a 'molecular fingerprint' demonstrated for use in various biomedical diagnostic applications. The technique allows for classification of both healthy tissue types and the discrimination of healthy versus diseased tissue, and can be a powerful tool for the diagnosis of disease [1-5]. Challenges still exist, however, in performing Raman spectroscopic measurements below the skin surface *in vivo*. Conventional Raman spectroscopy is limited in non-transparent turbid media to studying the sample surface, due to the inability to focus or confocally collect sufficient light at depths beyond a few tens of μm below the surface. Raman measurements in tissues are restricted in depth of penetration as well as in sensitivity and limit of detection due to multiple diffuse scattering events, light absorption by various tissue components, and the fluorescent background and Raman signal from the surface and bulk overwhelming the Raman signals of diagnostic interest [6-8].

The majority of biomedical Raman spectroscopy thus far has been performed in tissue specimens *ex vivo*. Deep Raman techniques such as SORS (Spatially Offset Raman Spectroscopy) [9], Transmission Raman Spectroscopy (TRS) [10], and TRRS (Time Resolved Raman Spectroscopy) [11, 12] have demonstrated potential to go *in vivo* [13]. These techniques allow for Raman spectroscopic measurements of bulk materials at limited depths (mm-cm scale) within tissues and other opaque, light-scattering materials by relying on the scattering properties of the material to provide a spatial or temporal discrimination between surface signals and depth signals.

The promise of non-invasive diagnostic techniques via these methods is very appealing, however, penetration depth, sensitivity, and precise depth selectivity when measuring from the skin surface is limited, due to the complex interaction of light with tissues. An alternative option for applying Raman techniques *in vivo* is to use a sub-cutaneous fibre optic probe directly in the region of interest within the body [14-25]. Such probes include Raman-based endoscopes and catheters that can probe the surface of hollow organs of the body, and recently a fibre optic probe was designed that can be inserted subcutaneously via a hypodermic needle [25]. This needle probe design consisted of one excitation and one collection fibre in a bevelled tip, and was shown to have the sensitivity to discriminate tissue types as well as metastatic malignant disease in excised lymph

nodes *ex vivo* [25].

Here we present the next generation of Raman needle probe, which provides increased collection efficiency through additional collection fibres. The bevelled tip of the previous 2-fibre prototype was built to sample as close to the needle tip as possible [25]; this approach can be ideal for accurate tissue localisation at the needle tip. However, for those applications where larger sampling volumes may be required, the probe design has been modified such that the tip face of the Raman needle probe presented here is flat. The flat polished tip allows for a relatively larger sampling volume [26,27], and combined with increased collection fibres, a significantly improved SNR in measuring biological samples as compared with the 2-fibre needle probe.

The work outlined in this paper was motivated by the clinical need for making a rapid, minimally invasive diagnosis of Hodgkin's and Non-Hodgkin's lymphoma [28]. Such an approach requires the measurement of abnormal lymph nodes, buried below the skin surface, to enable the Raman molecular signals associated with disease to be interrogated for identification of metastatic lymph nodes. The needle probe design will allow for some form of bulk sampling within the lymph node of interest which is ideal for studying the macro-chemistry. Lymph nodes can be highly heterogeneous, and a bulk sampling provides a mean spectrum of the lymph node with a higher probability of contribution to the signal from diseased tissue over point spectra collected from a small area [29,30].

Current gold standard methods for the diagnosis of lymphomas include a needle biopsy or excision of the lymph node, followed by classification by a histopathologist. We aim to develop a clinical diagnostic tool that will be less invasive than surgical biopsy, and provide an immediate diagnosis based upon molecular signals, thus providing greater efficacy in diagnosis than the current gold standard techniques [28]. This procedure would clearly reduce patient stress and limit the number of unnecessary surgeries.

Materials and Methods

Ethics

Excised human lymph nodes used in this study were collected and measured with informed written consent of the donors, who were undergoing routine surgical procedures. Ethical approval has been provided by the Gloucestershire Local Research Ethics Committee.

Instrumentation

Multi-fibre probe tip design

As shown in detail in Figure 1, the probe tip is composed of a bundle of low-OH silica optical fibres (0.22 NA, Thorlabs) with 105 µm diameter cores and 125 µm silica cladding. The 250 µm acrylate buffer coating was first stripped from the fibres, and then they were fixed together with a biomedically-approved epoxy into a custom-cut piece of stainless steel tubing (Hamilton, 22 gauge). The bundle was polished flat, arranged in an orientation of 6 collection fibres around 1 excitation fibre. This configuration is very similar to many probes designed for clinical application, the differences being that the overall diameter of this probe (720 µm) allows it to be inserted and move freely back and forth inside a 19 gauge disposable hypodermic needle, and that the expensive and complex filters and optics are left outside of the needle probe tip. The length of unfiltered fibre bundle in the needle probe tip is relatively low cost, enabling this portion to be disposable.

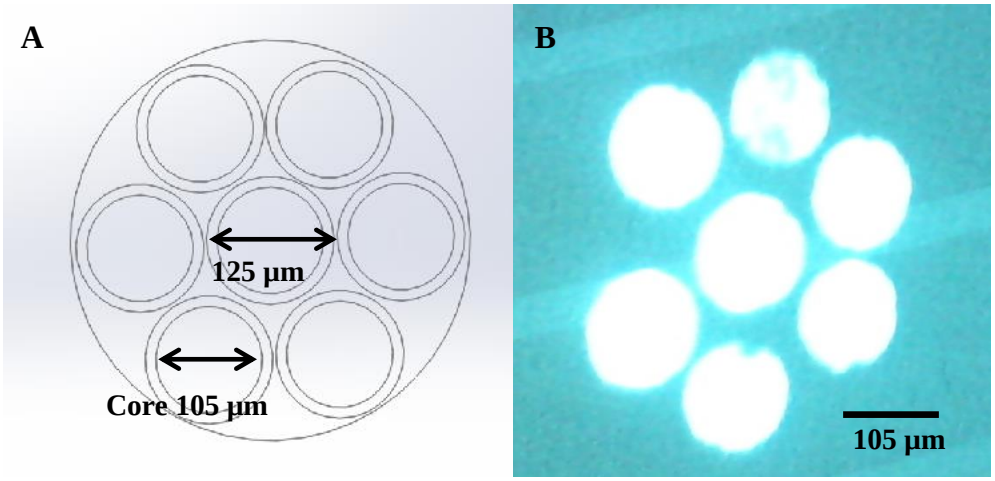

C

Fibre diameter	Probe ID /OD	Probe gauge	Outer needle gauge	# of fibres	Area of collection
125 µm	**410/720 µm**	**22**	**19**	**7**	**5.19×10^4 µm^2**
220 µm	**686/1070 µm**	**19**	**16**	**7**	**1.88×10^5 µm^2**

Fig. 1. (A) Design of the probe tip with 6 collection fibres around 1 excitation fibre using fibres with 125 µm outer diameter (including cladding) and 105 µm core, encased in a stainless steel tube (22 gauge, 720µm outer diameter (OD), 410 µm inner diameter (ID)). (B) A magnified probe tip after polishing with white light illumination of the fibre cores. (C) Collection areas of 6 around 1 orientations of 125 µm and 220 µm fibres inside standard tube gauge sizes (ID and OD are shown), where A=summed area of collection of the fibre cores for n-1 fibres, where n is the

total number of fibres, for a given design. ‘Outer needle gauge’ refers to the smallest size hypodermic needle tip that the probe fits inside [31].

The needle tip of the probe can be made to any length; the constraints are that the Raman background from unfiltered silica fibre increases with increasing fibre length in the needle tip. The human anatomy leads to the requirements for a maximum needle length of ~10 cm. As outlined above our primary medical interest is in studying lymph nodes of the head and neck area with this instrument, and a needle length of ~6 cm was confirmed by head and neck surgeons as being a sufficient and medically-relevant depth to reach below the surface tissues.

In theory, the greater the collection area: the larger the signal obtained by the probe. This can be achieved with more fibres or fibres with larger cores. However, in practice, the addition of extra collection fibres may not be necessary if the required SNR for spectral discrimination is achievable with fewer collection fibres. There exists a trade-off between maximum collection area (number or size of fibres) and total needle diameter acceptable to the patient; a smaller needle appears less daunting, but may require longer measurement time than a slightly broader needle with greater collection area. The respective collection areas provided by 125 µm and 220 µm fibres in 6 around 1 orientations inside standard needle gauge sizes are shown in Figure 1 C. Although various options, such as using 220 µm fibres, give a larger total collection area than the 6 around 1 fibre design using 125 diameter fibres, the needle diameter also increases considerably in these cases. There is also diminishing advantage in using larger fibres as they couple less efficiently into the spectrometer.

Raman needle probe instrumental setup

A schematic of the multifibre Raman needle probe instrument is depicted in Figure 2. Excitation at 830 nm is delivered by an IPS spectrum stabilized laser module (Innovative Photonic Solutions, I0830MM0350MF), passing through a collimating lens and short-pass filter (BrightLine® FF01-830/2-25, Semrock, Rochester, NY, USA) via a 105 µm core fibre optic patch cable, and is launched into the centre fibre (105 µm core/125 µm graded index low-OH silica fibre, Thorlabs) of the needle tip bundle. Excitation power was adjusted between 20 mW and 100 mW depending on the sample requirements. The specific excitation power used in each measurement is indicated in the corresponding figure caption.

Light is collected at the needle tip via the 6 collection fibres (105 µm core/125 µm graded index

low-OH silica fibre, Thorlabs) encircling the excitation fibre, as depicted in Figure 1. In these experiments the fibre collections were intentionally measured separately, i.e. a single fibre of the bundle was selected for collection at a time, and paired lenses with FC connectors were used (Thorlabs, 0.26 NA F220FC-780 nm) to pass the collected light through a long-pass filter (RazorEdge®, LP02830RU-25, Semrock, Rochester, NY, USA). The collected light is then launched into fibres that terminate in a vertical column over the 6 mm length of the entry port of the spectrometer (Raman Explorer 830, 1002A-00465, Headwall Photonics, Fitchburg, MA, USA). The spectrometer is coupled to a deep-depletion Charge-Coupled Device (CCD) camera (iDus, DU420A-BR-DD, Andor, Belfast, UK).

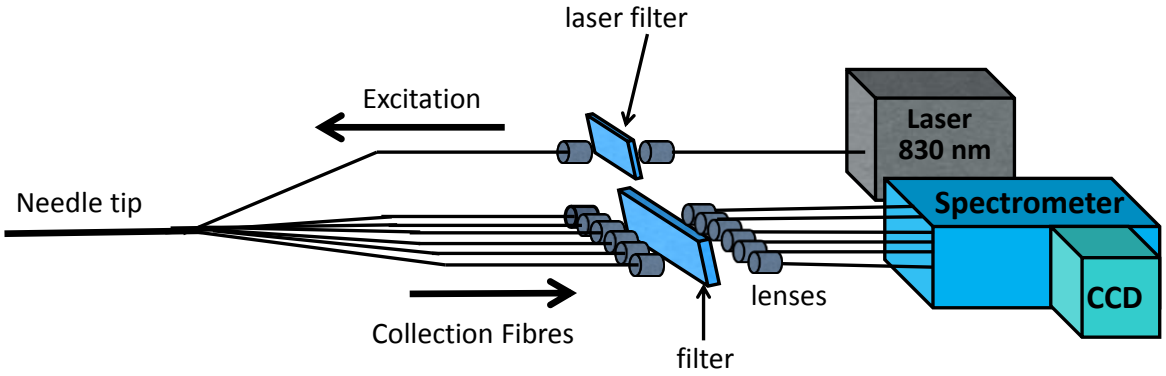

Fig. 2. Schematic diagram depicting the Raman needle probe instrumental setup. Excitation at 830 nm was provided by a CW IPS laser passing via fibre optic cable through a short pass filter ('laser filter'), and into the central fibre of the needle tip. The six collection fibres returning from the needle tip were directed through a long pass filter ('filter') and were delivered to the spectrometer in a vertical column across the entry port. Spectra were acquired with a deep depletion CCD camera.

Experimental Methods

Measuring sampling depth in tissue phantoms

The sampling depth of the Raman needle probe was measured in a two-layer tissue phantom, using the instrument depicted in Figure 2 and experimental setup shown in Figure 3A. The phantom consisted of a 2 mm-thick piece of Polytetrafluoroethylene (PTFE) in the bottom of a petri dish filled with a scattering liquid (see Figure 3).

PTFE is a white scattering plastic with a similar refractive index and scattering to tissue [32,33]. It provides a distinct Raman signal that can be used to demonstrate the depth of probing in tissue-simulating phantoms. The Raman cross section of PTFE is generally larger than biological tissue,

but the SNR of PTFE spectra is more comparable to that of tissue than many other common polymers with even larger Raman cross sections.

Solutions with varying concentrations of Intralipid ® (IL) (Sigma-Aldrich, 20%) in water were used as the scattering liquid, and were formulated in a range of scattering concentrations of 0.5%, 1%, and 20% IL by volume. IL is frequently used as a scattering agent in tissue-simulating phantoms, and its optical properties have been well characterized at various wavelengths [34-38]. Of the concentrations used, near 1% IL most resembles the scattering at 830 nm of soft, adipose-rich biological tissue similar to lymph nodes ($\mu_{s'}$ of ~1-10 cm^{-1}) [39-41], while the highest scattering concentration of 20% IL scatters more strongly than biological tissues at this wavelength ($\mu_{s'}$ of ~100 cm^{-1}).

The probe was placed on a micrometer z-stage and the needle tip was positioned in the scattering liquid of the tissue phantom with the tip face touching the surface of the PTFE. The probe was then raised vertically away from the PTFE within the scattering liquid in steps of 50 µm, recording Raman spectra at each step consecutively. Spectral acquisition time for all sampling depth measurements was 1s x 10 accumulations.

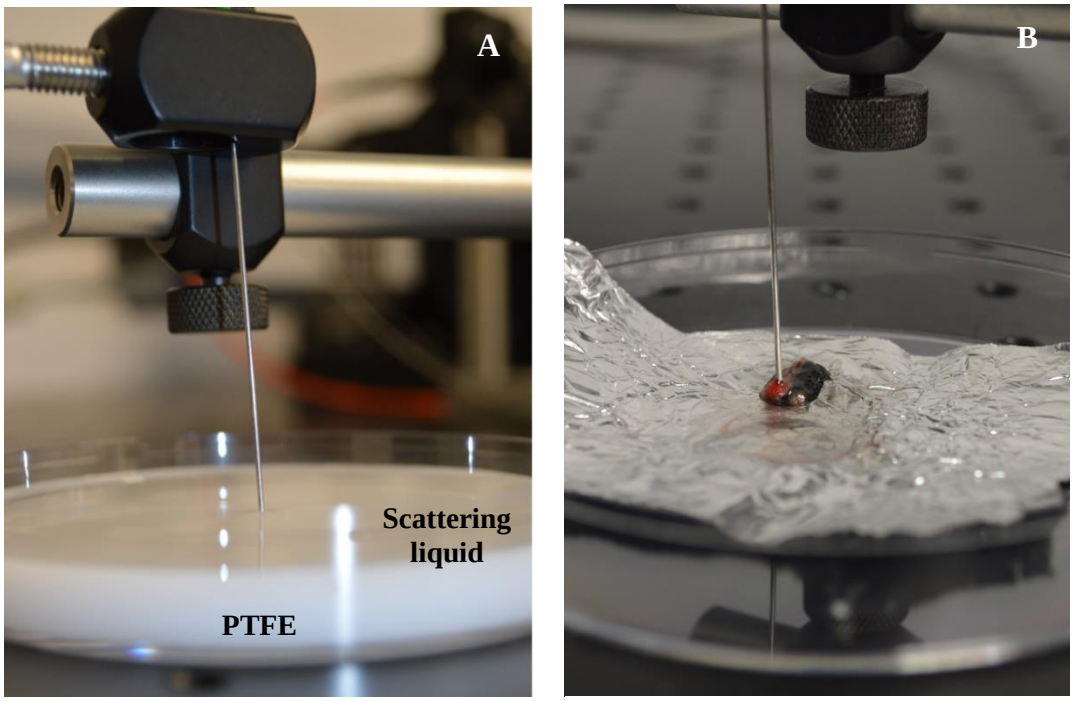

Fig. 3. Photos of (A) the sampling depth measurements in PTFE and IL phantoms, and (B) of measurements of an excised human lymph node (mediastinal) on top of aluminium foil.

Addition of absorption to tissue phantoms

An additional sampling depth experiment was performed in which India ink (American MasterTech Scientific, Inc., Lodi, CA, USA) was added to the scattering liquid as an absorbing agent. India ink is particularly appropriate as a light absorber in biological tissue phantoms because it is easy to incorporate homogenously into various media, including IL solutions, and it has a well-characterized broadband absorption spectrum [37,38,40,42,43]. The ink was commercially available as a stock solution of unknown concentration. It was first characterized by UV-Vis absorption of a series of dilutions of the stock solution, from which a 0.2 µl/ml solution of India ink was determined to have an absorption coefficient (μ_a) of ~0.05 mm^{-1} at 830 nm. The India ink solutions were sonicated prior to the UV-Vis measurements, and also after addition to the scattering liquid in the phantom, to ensure the ink particles were homogenously dispersed.

Measurements of human lymph node tissue

The target application of this probe will be *in vivo* Raman measurements in lymph nodes, which have a more heterogeneous consistency than tissue phantoms. As previously noted, while PTFE has similar elastic scattering properties to tissue, the Raman cross-section of PTFE is generally larger than that of most biological tissues. A stronger Raman signal from PTFE could result in an over-estimation of the sampling volume compared to that expected of this probe in biological tissue, due to the higher signal providing an increased limit of detection.

In addition, it is important to verify that the optical values we have selected for our phantoms based on various reported literature values do in fact match up well with real lymph node tissue. Using a phantom with a much higher scattering coefficient may result in an underestimation of the sampling depth that would be expected in lymph node tissue, and using much lower scattering values may also provide significantly different results.

To verify the appropriateness of the phantom materials used in this study, we also performed sampling depth experiments with a human lymph node sample of ~0.5 cm thickness placed on top of PTFE. This two-layer sample was measured by the same procedure and under the same conditions as used for PTFE and IL phantoms described previously.

Results and Discussion

Sampling depth in phantoms

Figure 4 depicts PTFE signal decay curves as measured with increasing distance of the Raman needle probe to the PTFE surface, within an IL phantom. The decay in net peak height of a representative peak of PTFE (730 cm^{-1} PTFE peak intensity with the baseline signal next to the peak subtracted) was plotted versus distance of the probe surface from the PTFE. Measurements were taken in increments of 50 µm, moving the probe through the IL phantom medium up to 1 mm separation of probe and sample (PTFE). This signal decay profile was plotted for various phantoms, with different concentrations of IL and India ink, as shown in Figure 4.

With increasing scattering concentration, the slopes of the decay curves became steeper, and the signal intensity also increased, due to the greater number of photons undergoing multiple scattering events and thus reaching the detection fibres, while in the lower scattering phantoms a lower fraction of light is backscattered.

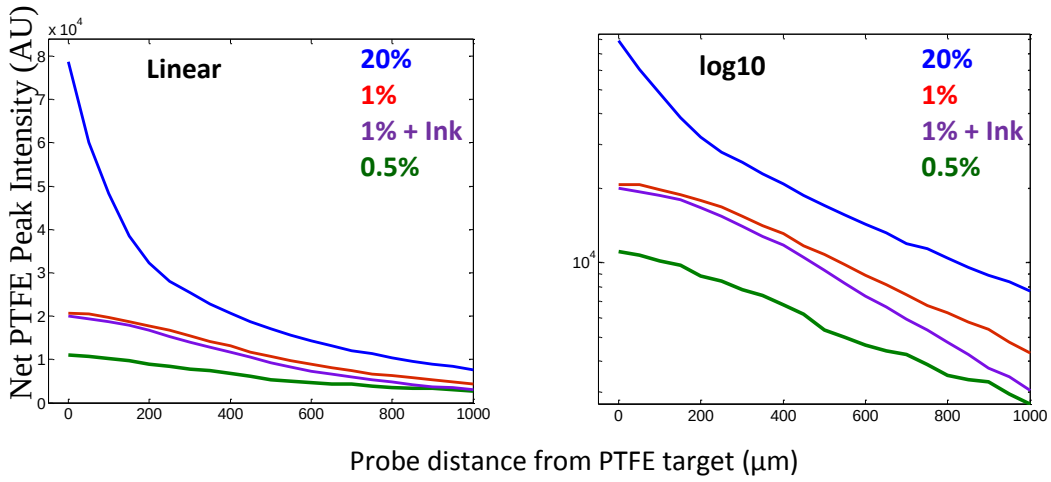

Fig. 4. The decay in net peak height of a representative peak (730 cm^{-1}) of a PTFE layer within scattering liquid phantoms with increasing probe distance from the PTFE, as measured with the Raman needle probe. Different scattering liquid phantoms were used; 0.5%, 1% plus 0.2 µl/ml India ink, 1% and 20% IL in water. Profiles are listed in order from top to bottom, and are plotted on linear and log10 y-axis scales. Spectra were acquired for 1 s x 10 using 830 nm excitation at 100 mW, in consecutive measurements increasing the probe distance from the PTFE in steps of 50 µm.

Sampling depth in lymph nodes

In addition, the decay of the Raman signal from a layer of PTFE was measured using an excised lymph node as the scattering medium. In Figure 5, the PTFE beneath lymph node decay profile is

compared to the PTFE decay profile measured in the phantom of 1% IL and 0.2 µl/ml India ink discussed in the previous section.

Practical constraints from the small size and inhomogeneity of the excised lymph node resulted in a profile that was only measured over a range of 300 µm; however the general signal decay trend is still evident over this shorter range. It appears from these plots that the scattering and absorption of the lymph node measured are greater than that used in the liquid phantom (where the value used was based on the literature). It is known that this node contains many soot particles accumulated from the filtering of the lymphatic fluid around the lungs of the donor, which may have had a significant contribution to the absorption.

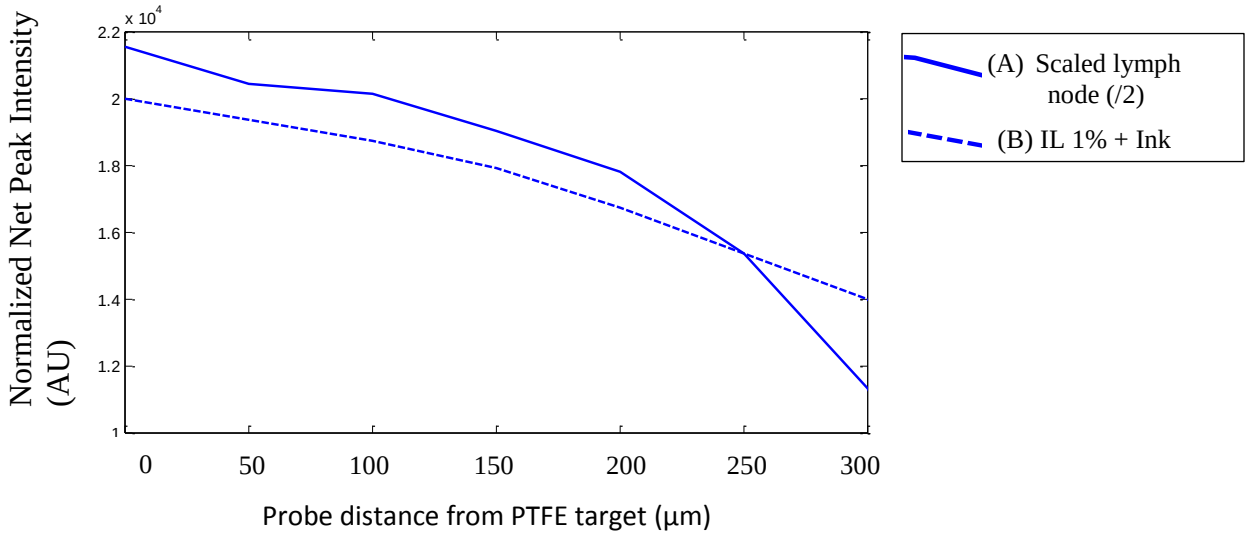

Fig. 5. Decay profile of PTFE from sampling volume measurements using (A) PTFE signal through lymph node over 300µm distance, and (B) PTFE signal in a liquid phantom of 1% IL and 0.02µl/ml India ink solution. The range of the decay profile measurements is limited by lymph node size and inhomogeneity, and the phantom measurement is shown over the same range for comparison.

2-fibre vs multi-fibre probe for disease discrimination

The bevelled tip of the 2-fibre needle probe provided a smaller sampling volume than the flat tip probe, and thereby also lower signal intensity. The addition of multiple collection fibres also improves the SNR of spectra collected with the flat tip probe. An illustration of the effect of combining signal from multiple collection fibres can be seen in Figure 6 for PTFE and for excised human lymph node. Spectra from the 6 collection fibres are shown individually in Figure 6 A and C and their combined collection is shown in Figure 6 B and D. While there are minor differences in the spectra from individual fibres (+/- 4% on average) these can be attributed to differences in

the silica background due to differences in cleaving, polishing and connections of each individual collection fibre to the spectrometer; as well as to slight variations in fibre length. While there is also small variation in distance of the individual collection fibres to the central excitation fibre, this variation is on the order of 5 µm, and was found to have a negligible effect on signal intensity given the sampling volume and scattering nature of the samples. This was supported by results from Monte-Carlo simulations (results not shown).

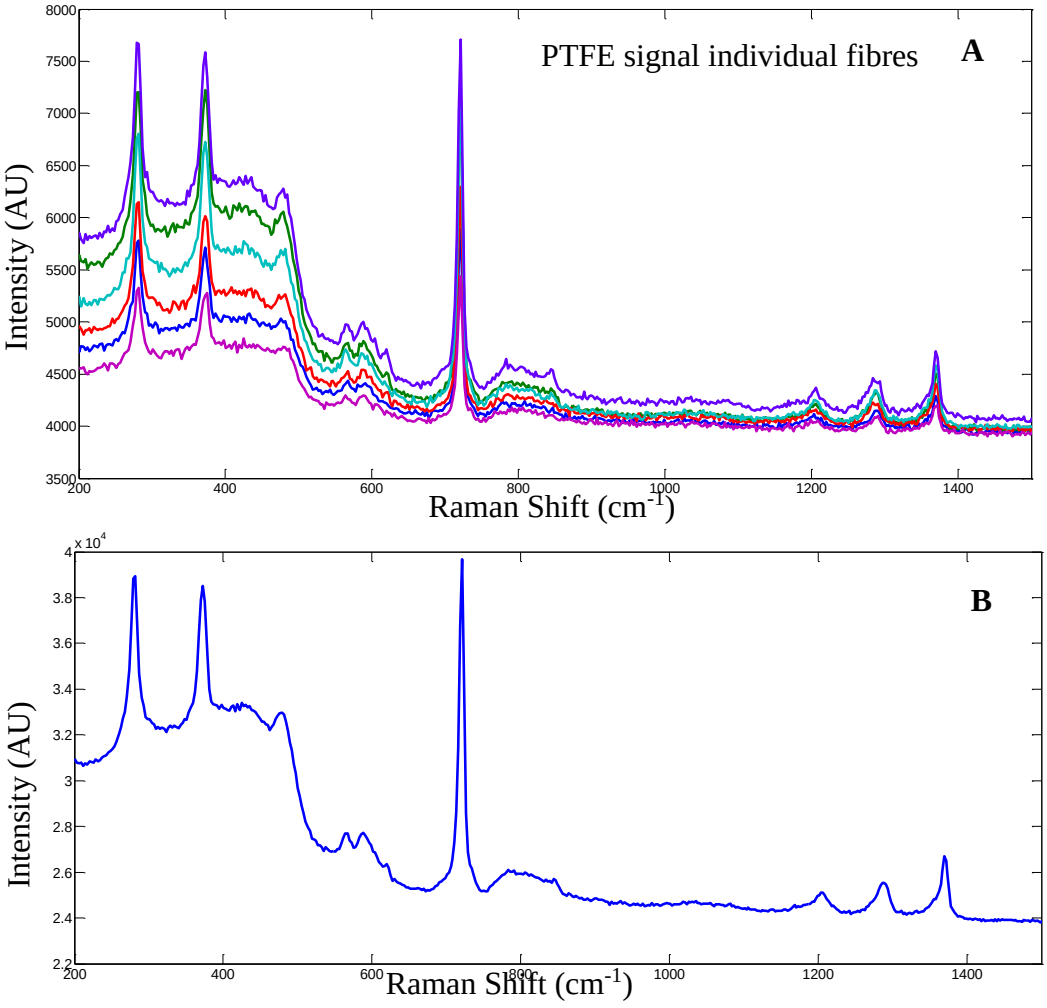

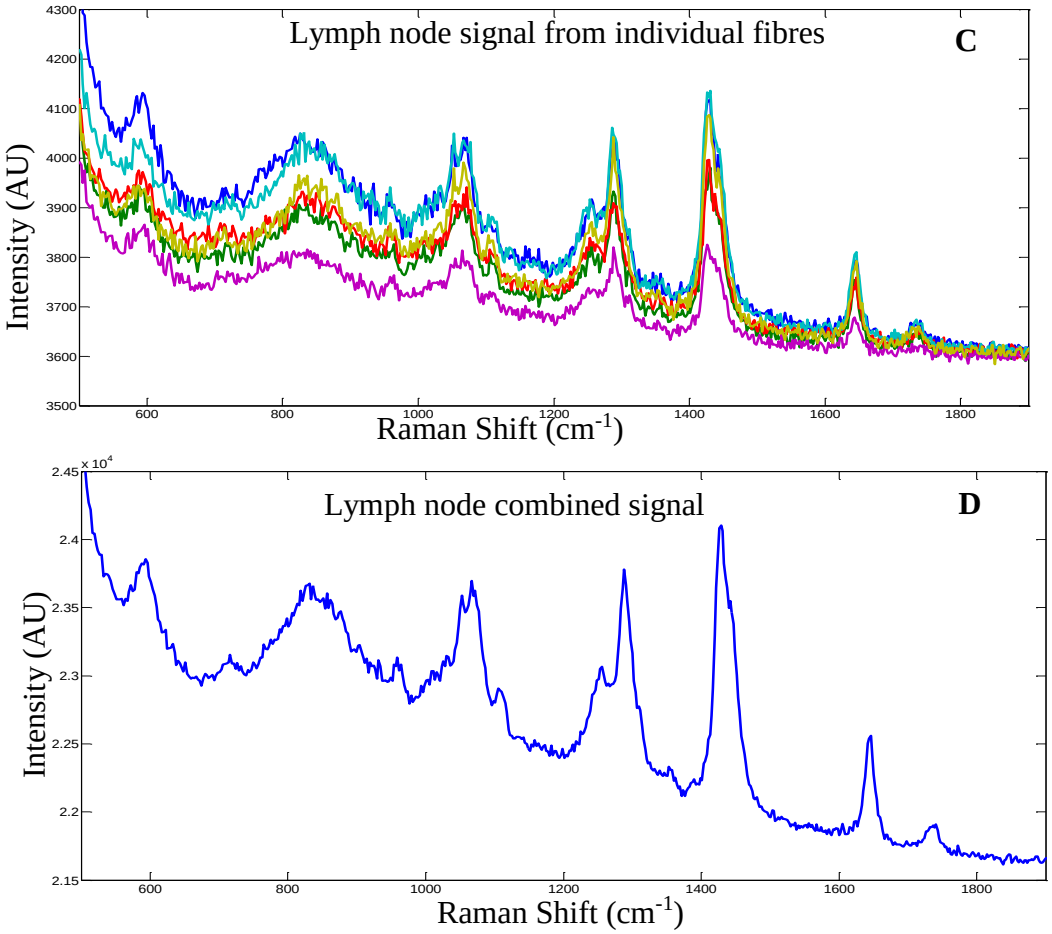

Fig. 6. Spectra from the Raman needle probe: (A) Spectra of PTFE from individual collection fibres 1-6, (B) combined spectral collection of PTFE from all 6 fibres. C) Raw spectra of excised lymph node tissue from individual fibres 1-6, (D) combined spectral collection of excised lymph node tissue from all 6 fibres. Spectra were acquired for 5s x 1 at 830 nm, excitation power at the sample was 20 mW. Data shown is unprocessed.

Table 1. SNR obtained from this study in comparison to our previous work (as measured by [max. Amide I peak height-mean of background]/RMS noise of background). SNRs shown for individual fibre collection, combined fibre collection from the multi-fibre Raman needle probe (MFNP); lymph node spectra measured with Raman microscopy from Lloyd *et al*.(2013)[28]; and in a lymph node spectrum measured with the 2-fibre bevelled tip probe from Day and Stone (2013)[25]. In all cases, spectral acquisition was 5s x 1, 830 nm, 20 mW, except lymph node data from Day and Stone (2013)[25], (which used 30s x 1, 830 nm, 24 mW). It should be noted that a different spectrometer, laser and CCD were used to obtain the data in these three instrumental scenarios.

	SNR lymph node Amide I (1650 cm^{-1} / RMS Noise)	SNR PTFE (1370 cm^{-1} / RMS Noise)
MFNP Individual fibre spectra	15.07 (+/- 5.29)	34.77 (+/- 9.54)

MFNP Additive spectrum of fibres 1-6	*37.46*	*84.71*
Day and Stone (2013) 2-fibre probe with bevelled tip.	*16.06 (+/- 14.76)* *(30s, 830 nm, 24 mW)*	*45.98 (+/- 2.56)*
Spectra from Lloyd, *et al.* (2013)	*10.59 (+/- 7.24)*	*N/A*

A comparison of SNRs of PTFE and lymph node measurements made with the single and multiple collection fibre needle probes is summarized in Table 1. SNRs of Raman data from lymph nodes measured with the two-fibre probe (from Day and Stone, 2013 [25]), and a different CCD, laser, spectrometer, and measurement parameters, are also shown for a rough comparison. It should be noted that differences in composition between the lymph nodes measured may also contribute to the differences in SNR, rather than just probe efficiency.

The new multi-fibre probe appears to provide higher SNR in lymph nodes, and higher SNRs in measuring the surface of PTFE, than the previous bevelled tip, two-fibre probe. However, for single fibre comparisons, the bevelled tip sampled the PTFE signals in air more efficiently. It is important to note that the scattering and Raman cross section of PTFE is higher than those of lymph nodes, and the two probe designs behave differently if they are measuring scattering surfaces in air, versus being completely immersed in a scattering material (tissues and phantoms). The bevelled tip probe collects efficiently from a small volume at the probe tip, and will therefore most efficiently collect Raman photons created at the illumination point. The individual flat tipped fibres of the multi-fibre probe will sample less efficiently at the surface as the collection zone is offset by 125 μm from the illumination zone. This inherently reduces the surface signal collected, but increases the relative number of photons collected that originated from greater depths than the first few 10s μms. Moving the flat tip multifibre probe slightly away from the surface of a scattering or reflective sample in air gives an improved signal from distance 0, as more backscattered Raman photons then fall within the collection angle. When the flat probe tip is completely immersed in a scattering medium, the surrounding medium serves to backscatter these photons to a collection fibre.

In previous work by Lloyd, *et al.* [28], multivariate analysis was used to discriminate benign, primary, and secondary malignancies in lymph nodes with 81% sensitivity and 89% specificity using Raman microscopy data. Based on this data, a rough estimation can be made on the target SNR that would be required of a clinical probe to achieve sufficient discrimination of lymph node pathologies. Using the Amide I peak (~1650 cm^{-1}) the multi-fibre needle probe evaluated here achieves sufficient SNR from lymph node spectra, using a single collection fibre, to exceed that used for discrimination by Lloyd *et al*. The combined six-fibre signal was shown to provide approximately 3-4x the SNR required for lymph node discrimination in the above paper. This suggests that using the current probe design with six-fibre collection would provide sufficient signal for pathology discrimination with 20 mW power in between one and two seconds.

Conclusions

A flat tipped probe utilizing multiple collection fibres inside a hypodermic needle provides improved overall signal collection efficiency in lymph nodes compared with the previous 2-fibre probe design. Utilizing all collection fibres of the probe gives an improvement in SNR of around 2.5 times over that achieved with single fibre collection.

The collection efficiency of a single fibre in the flat probe tip is lower than an equivalent bevelled tip when coupling to a scattering sample of PTFE in air. The multi-fibre probe with flat tip collects photons more efficiently and from a larger volume than the bevelled tip probe when submerged in scattering materials such as tissue phantoms or human tissues; Monte-Carlo simulations additionally support this conclusion (see Electronic Supplementary Material Fig. S1). The later measuring scenario is most relevant to the biological sampling necessary for clinical use of this probe.

While the Raman needle probe with more collection fibres has a slightly larger overall needle diameter than the previous 2-fibre version, the improvement in SNR will allow for quicker measurements to make diagnostic discrimination. This instrument is much less invasive than surgical excision of lymph nodes, or core needle biopsy utilizing a standard biopsy needle of 1.8 mm diameter.

We have measured the sampling depth of this probe in tissue phantoms, and have demonstrated that these phantoms are an appropriate model for lymph node tissue by performing comparative measurements in excised lymph nodes; phantom design should closely match the optical properties

of the tissue target. Sampling from a relatively large volume of the lymph node will be appropriate for diagnostic purposes [29,30].

While the new needle probe has multiple collection fibres, the measurements presented here were acquired with each collection fibre individually to study and account for any variation in signal from the different individual fibres. Some variations in signal intensity in the individual fibre spectra are observed, however this difference is most evident in the silica background (+/-4%). The spectral differences have not been shown to correspond with slight differences in distance between the collection and excitation fibres in the tip, which are expected to have a negligible effect on the SNR given the sampling volume of our probe. This was also verified by Monte Carlo simulations (data not shown).

The performance of the multi-fibre probe has been shown to be sufficient to provide Raman SNRs from lymphoid tissues (within 5s with 20mW 830nm illumination) in excess of those demonstrated elsewhere to discriminate lymph node pathologies. This leads us to conclude that similar discrimination to that in Lloyd *et al.* [28] should be possible *in vivo* in 1-2s with the same illumination.

Acknowledgements

The authors would like to thank Martha Vardaki for India ink characterization, and Gloucester Hospitals NHS Foundation Trust for providing the excised human lymph node tissue. This work is funded by a UK National Institute for Health Research (NIHR) Invention for Innovation (i4i) grant number II_LA_1111_20007.

References

1. Ellis DI, Cowcher DP, Ashton L, O'Hagan S, Goodacre R (2013) Illuminating disease and enlightening biomedicine: Raman spectroscopy as a diagnostic tool. Analyst 138(14):3871-3884

2. Talari ACS, Movasaghi Z, Rehman S, Rheman IU (2014) Raman Spectroscopy of Biological Tissues. Appl Spectrosc Rev 50: 46–111

3. Carden A, Morris MD (2000) Application of vibrational spectroscopy to the study of mineralized tissues (review). J Biomed Opt 5(3): 259–268

4. Hanlon EB, Manoharan R, Koo T-W, Shafer KE, Motz JT, Fitzmaurice M, Kramer JR, Itzkan I, Dasari RR, Feld MS (2000) Prospects for in vivo Raman Spectroscopy. Phys Med Bio 45(2):R1-R59

5. Stone N, Kendall C, Shepherd N, Crow P, Barr H (2002) Near-Infrared Raman Spectroscopy for the Classification of epithelial pre-cancers and cancers. J Raman Spectrosc 33:564-573

6. Matousek P, Morris MD, Everall N, Clark IP, Towrie M, Draper E, Goodship A, Parker AW (2005) Numerical simulations of subsurface probing in diffusely scattering media using spatially offset Raman spectroscopy. Appl Spectrosc 59(12):1485- 1492

7. Everall N, Hahn T, Matousek P, Parker AW, Towrie M (2004) Photon migration in Raman spectroscopy. Appl Spectrosc 58(5):591-597

8. Matousek P, Stone N (2009) Emerging concepts in deep Raman spectroscopy of biological tissue. Analyst 134:1058-1066

9. P. Matousek P, Clark IP, Draper ERC, Morris MD, Goodship AE, Everall N, Towrie M, Finney WF, Parker AW (2005) Subsurface Probing in Diffusely Scattering Media Using Spatially Offset Raman Spectroscopy. Appl Spectrosc 59(4):393-400

10. Matousek P, Stone N (2008) Advanced Transmission Raman Spectroscopy: A Promising Tool for Breast Disease Diagnosis. Cancer Res 68:4424

11. Matousek P, Everall N, Towrie M, Parker AW (2005) Depth Profiling in Diffusely Scattering Media Using Raman Spectroscopy and Picosecond Kerr Gating. Appl Spectrosc 59(2):200-205

12. Iping Petterson IE, Dvořák P, Buijs J, Gooijer C, Ariese F (2010) Time-resolved spatially offset Raman spectroscopy for depth analysis of diffusely scattering layers. Analyst 135(12):3255-3259

13. Matousek P, Stone N (2013) Recent advances in the development of Raman spectroscopy for deep non-invasive medical diagnosis. J Biophotonics 6(1):7–19

14. Draga ROP, Grimbergen MCM, Vijverberg PLM, van Swol CFP, Jonges TGN, Kummer JA, Bosch JLHR (2010) *In vivo* bladder cancer diagnosis by high-volume Raman spectroscopy. Anal Chem 82:5993–5999

15. Magee ND, Villaumie JS, Marple ET, Ennis M, Elborn JS,| and McGarvey JJ (2009) Ex vivo diagnosis of lung cancer using a Raman miniprobe. J Phys Chem B 113:8137–8141

16. Matthäus C, Dochow S, Bergner G, Lattermann A, Romeike BFM, Marple ET, Krafft C, Dietzek B, Brehm BR, Popp J (2012) *In vivo* characterization of atherosclerotic plaque depositions by Raman-probe spectroscopy and in vitro coherent anti-stokes Raman scattering microscopic imaging on a rabbit model. Anal Chem 84:7845−7851

17. Agenant M, Grimbergen M, Draga R, Marple E, Bosch R, van Swol C (2014) Clinical superficial Raman probe aimed for epithelial tumor detection: Phantom model results. Biomed Opt Express 5(4):1203-1216

18. Almond LM, Hutchings J, Kendall C, Day JCC, Stevens OAC, Lloyd GR, Shepherd NA, Barr H, Stone N (2012) Assessment of a custom-built Raman spectroscopic probe for diagnosis of early oesophageal neoplasia. J Biomed Opt 17(8):081421

19. Shim MG, Wilson BC, Marple E, Wach M (1999) Study of fibre-optic probes for in vivo medical Raman spectroscopy. Appl Spectrosc 53(6):619-627

20. Huang Z, Zeng H, Hamzavi I, McLean DI, Lui H (2001) Rapid near-infrared Raman spectroscopy system for real-time in vivo skin measurements. Opt Lett 26(22):1782-1784

21. Komachi Y, Katagiri T, Sato H, Tashiro H (2009) Improvement and analysis of a micro Raman probe. Appl Opt 48:1683-1696

22. Mahadevan-Jansen A, Mitchell MF, Ramanujam N, Utzinger U, Richards-Kortum R (1998) Development of a fiber optic probe to measure NIR Raman spectra of cervical tissue *in vivo*. Photochem Photobiol 68:427–31

23. Shim M, Song LMWK, Marcon NE, Wilson BC (2000) *In vivo* near-infrared Raman spectroscopy: demonstration of feasibility during clinical gastrointestinal endoscopy. Photochem Photobiol 72(1):146-150

24. Utzinger U, Richards-Kortum RR (2003) Fiber optic probes for biomedical optical spectroscopy. *J Biomed Opt* 8(1):121–147

25. Day JCC, Stone N (2013) A Subcutaneous Raman Needle Probe. Appl Spectrosc 67(3):349-354

26. Cooney TF, Skinner HT, Angel SM (1996) Comparative study of some fiber-optic remote Raman probe designs. Part II: Tests of single-fiber, lensed, and flat- and bevel-tip multi-fiber probes. Appl Spectrosc 50(7):849-860

27. Tai DCS, Hooks DA, Harvey JD, Smaill BH, Soeller C (2007) Illumination and fluorescence collection volumes for fiber optic probes in tissue. J Biomed Opt 12(3):034033-1

28. Lloyd GR, Orr LE, Christie-Brown J, McCarthy K, Rose S, Thomas M, Stone N (2013) Discrimination between benign, primary and secondary malignancies in lymph nodes from the head and neck utilising Raman spectroscopy and multivariate analysis. Analyst 138:3900-3908

29. Horsnell J, Stonelake P, Christie-Brown J, Shetty G, Hutchings J, Kendall C, Stone N (2010) Raman spectroscopy—A new method for the intra-operative assessment of axillary lymph nodes. Analyst 135:3042–3047

30. Horsnell JD, Smith JA, Sattlecker M, Sammon A, Christie-Brown J, Kendall C, Stone N (2012) Raman spectroscopy- A potential new method for the intra-operative assessment of axillary lymph nodes. the Surgeon 10:123-127

31. The Engineering Toolbox. http://www.engineeringtoolbox.com/smaller-circles-in-larger-circle-d_1849.html Accessed 9 December 2014.

32. Sadhwani A, Schomacker KT, Tearney GJ, Nishioka NS (1996) Determination of Teflon thickness with laser speckle. I. Potential for burn depth diagnosis. Appl Opt 35(28):5727-5735

33. Iping Petterson IE, Ariese F (2012) Time-Resolved Raman Spectroscopy for Non-invasive detection through non-transparent materials. Spectroscopy Europe 24(1):19-21

34. Aernouts B, Van Beers R, Watté R, Lammertyn J, Saeys W. (2014) Dependent scattering in Intralipid® phantoms in the 600-1850 nm range. Opt Express 22(5):6086-6098

35. Royston DD, Poston RS, Prahl SA (1996) Optical properties of scattering and absorbing materials used in the development of optical phantoms at 1064 nm. J Biomed Opt 1(1): 110-116

36. Di Ninni P, Martelli F, Zaccanti G (2011) Intralipid: towards a diffusive reference standard for optical tissue phantoms. Phys Med Biol 56:N21–N28

37 Spinelli L, Botwicz M, Zolek N, Kacprzak, M, Milej, D, Liebert, A, Weigel, U, Durduran, T, Foschum, F, Kienle, A, Baribeau, F, Leclair, S, Bouchard, J-P, Noiseux, I, Gallant, P, Mermut, O, Pifferi, A, Torricelli, A, Cubeddu, R,. Ho, H-C, Mazurenka, M, Wabnitz, H, Klauenberg, K, Bodnar, O, Elster, C, Bénazech-Lavoué, M, Bérubé-Lauzière, Y, Lesage, F, Di Ninni, P, Martelli, F, Zaccanti,G (2012) Inter-Laboratory Comparison of Optical Properties Performed on Intralipid and India Ink. Biomedical Optics, Optical Society of America BW1A-6

38. Pogue BW, Patterson MS (2006) Review of tissue simulating phantoms for optical spectroscopy, imaging and dosimetry. J Biomed Opt 11(4):0411021-04110216

39. Jacques SL (2013) Optical properties of biological tissues: a review. Phys Med Biol 58:R37-R61

40. Cubeddu R, Pifferi A, Taroni P, Torricelli A Valentini G (1997) A solid tissue phantom for photon migration studies. Phys Med Biol 42:1971–1979

41. Michels R, Foschum F, Kienle A (2008) Optical properties of fat emulsions. Opt Express 16(8):5907

42. Madsen SJ, Patterson MS, Wilson BC (1992) The use of India ink as an optical absorber in tissue-simulating phantoms. Phys Med Biol 31(4):985-993

43. Di Ninni P, Martelli F, Zaccanti G (2010) The use of India ink in tissue-simulating phantoms. Opt Express 18(26):26860